RSC Advances

PAPER

View Article Online
View Journal | View Issue

Cite this: *RSC Adv.*, 2019, **9**, 28102

Converse transitions between the micelles and the vesicles of pyrrolidone-based AIE amphiphilic copolymers in polar and apolar solvents†

Xiaolong He, Beibei Wang, Xuefeng Li * and Jinfeng Dong*

Herein, a new family of aggregation-induced emission (AIE) amphiphilic copolymers, named poly(*N*-(2-methacryloyloxyethyl)pyrrolidone)-*b*-poly(lauryl methacrylate-*co*-1-ethenyl-4-(1,2,2-triphenylethenyl) benzene), PNMP$_x$-*b*-P(LMA$_y$-*co*-TPE$_z$), was developed by the reversible addition–fragmentation chain transfer (RAFT) polymerization method. The polymerization degree *x* of the NMP segment was kept constant at 35, whereas that of the LMA segment ranged from 9 to 55 with the polymerization degree ratio *y*/*z* of the LMA and TPE segments being around 9. As a result, the PNMP$_x$-*b*-P(LMA$_y$-*co*-TPE$_z$) copolymer gradually transformed from being water soluble to oil soluble with an increase in the length of the P(LMA$_y$-*co*-TPE$_z$) segment. Moreover, these copolymers could form self-organized normal and reverse assemblies in both water and *n*-dodecane. Various morphologies, including spherical micelles, worm-like micelles and vesicles, were confirmed by the transmission electron microscopy (TEM) observation. Specifically, the micelle-to-vesicle transition *via* worm-like micelles occurred in the aqueous solution upon increasing the length of the P(LMA$_y$-*co*-TPE$_z$) segment, whereas the reverse transition occurred in *n*-dodecane. Because of the presence of the AIE-active TPE segment, both the aqueous and the *n*-dodecane solutions of PNMP$_x$-*b*-P(LMA$_y$-*co*-TPE$_z$) were highly luminescent, and their fluorescence quantum yields significantly depended on the polarity of the solvent and the morphology of the assemblies. Due to the strong luminescence properties of PNMP$_x$-*b*-P(LMA$_y$-*co*-TPE$_z$) assemblies, these AIE-active amphiphilic copolymers acted as excellent bioimaging probes with high efficiency.

Received 2nd August 2019
Accepted 22nd August 2019

DOI: 10.1039/c9ra05997k

rsc.li/rsc-advances

1 Introduction

Currently, studies on the application of luminescent probe molecules as cell imaging reagents, especially in biological systems, are attracting significant interest.[1–6] The development of highly efficient and biocompatible luminescent probes has been the key project.[7] However, the commonly presented aggregation-caused quenching (ACQ) phenomena have significantly limited and impeded the potential of the classic fluorescent molecules.[8] Alternatively, luminescent molecules processing anti-ACQ and showing aggregation-induced emission (AIE) can overcome the abovementioned shortcomings well.[9–11] Since the first report on the AIE phenomenon by the Tang's group in 2001,[12] the AIE effect has attracted significant attention; on the one hand, a series of AIE molecules has been developed based on the general luminescence mechanism that the AIE effect increases upon the restriction of intramolecular motion (RIM) including the restriction of both intramolecular rotation (RIR) and intramolecular vibration (RIV).[13–18] Moreover, the AIE phenomena have been applied in wide fields beyond the original imaging function. Note that AIE molecules with some particular amphiphilicity have always been in demand, which provide the primary driving force during the self-assembly processes. In other words, AIE molecules could be considered as amphiphiles containing some particular AIE-active moieties. As a result, numerous AIE molecules with interesting functions have been developed in recent years.[19–24]

The stability of amphiphilic copolymer assemblies is often more excellent than that of classic surfactants.[25] Accordingly, amphiphilic copolymers show promising potential in various application fields of biotechnology,[26] the development of functional materials,[27] drug-controlled release systems,[28] catalysis,[29] and so forth. Based on the classic synthetic methods such as the reversible addition–fragmentation chain transfer (RAFT) polymerization, atom transfer radical polymerization (ATRP), and nitroxide-mediated radical polymerization (NMR), numerous novel amphiphilic copolymers have been developed and their corresponding self-assembly behaviors have also been reported in the past few decades.[30–37] Recent studies on the polymerization-induced self-assembly (PISA) of amphiphilic

Engineering Research Center of Organosilicon Compounds & Materials, Ministry of Education, College of Chemistry and Molecular Sciences, Wuhan University, Wuhan 430072, P. R. China. E-mail: lixuefeng@whu.edu.cn; jfdong@whu.edu.cn

† Electronic supplementary information (ESI) available. See DOI: 10.1039/c9ra05997k

copolymers have attracted significant attention because the development of block copolymers and the preparation of aggregates with various morphologies have been simultaneously achieved, thereby further enriching the amphiphilic copolymers.[38–42]

Our group has reported some pyrrolidone-based amphiphilic diblock copolymers synthesized by the RAFT method for the first time; these copolymers not only show rich self-assembly behaviors in both polar and apolar solvents but also display some interesting stimuli-responses. For example, the micellization of poly(methacrylate acid)-*b*-poly(*N*-(2-methacryloyloxyethyl)pyrrolidone) (PMAA-*b*-PNMP) in the aqueous solution is sensitive to both pH and temperature that significantly benefits the development of gold nanoparticles with controlled size;[43] alternatively, their corresponding esterified products, *i.e.* poly(*N*-(2-methacryloyloxyethyl)-pyrrolidone)-*b*-poly(methyl methacrylate) (PNMP-*b*-PMMA), form organogels in isopropanol with thermally reversible transitions between 3D micellar networks and spherical micelles.[44] In a recent study, Armes and coworkers have reported the interesting assembly behaviors of pyrrolidone-based amphiphilic diblock copolymers in *n*-dodecane.[45] Recently, we have reported the detailed self-assembly behaviors of poly(*N*-(2-methacryloyloxyethyl)-pyrrolidone)-*b*-poly(lauryl methacrylate) (PNMP-*b*-PLMA) in *n*-dodecane,[46] where aggregates with rich morphologies, including spherical micelles, worm-like nanoparticles, and vesicles, can be formed by slightly changing the molar ratio of the PNMP and the PLMA segments. In addition, we have noticed interesting self-assembly behaviors of them in water. This suggests the promising self-assembly of PNMP-*b*-PLMA in both water and *n*-dodecane, and similar behaviors have been rarely reported previously for amphiphiles in two distinct solvents simultaneously. The introduction of an additional AIE-active segment into these particular amphiphilic copolymers might significantly extend the application potential of these coplymers.

In this study, a new family of the AIE amphiphilic copolymers PNMP$_x$-*b*-P(LMA$_y$-*co*-TPE$_z$), named poly(*N*-(2-methacryloyloxyethyl)pyrrolidone)-*b*-poly(lauryl methacrylate-*co*-1-ethenyl-4-(1,2,2-triphenylethenyl)benzene), was developed by the RAFT method. Their self-assembly behaviors in both water and *n*-dodecane were comprehensively studied by the dynamic light scattering (DLS), confocal laser scanning microscopy (CLSM) and transmission electron microscopy (TEM) techniques. Moreover, the structure–property relationship of PNMP$_x$-*b*-P(LMA$_y$-*co*-TPE$_z$) was established. Because of the presence of the TPE segment, these AIE-active amphiphilic copolymers could act as luminescent probes and were applied in bioimaging using HeLa cells as substrates.

2 Experimental

2.1 Materials

2-Cyano-2-propyl dithiobenzoate (CPDB) was synthesized according to a previously reported procedure.[47] 2,2′-Azobisisobutyronitrile (AIBN, 99%, Shanghai HATECH Co. Ltd.) was recrystallized from methanol. Methacryloyl chloride (98%, Shanghai HATECH Co. Ltd.) was distilled under reduced pressure prior to use. Lauryl methacrylate (LMA, 99%, TCI) was passed through a column of silica gel to remove the inhibitor. All other chemicals were used as received.

2.2 Synthesis of the PNMP-*b*-P(LMA-*co*-TPE) diblock copolymer

The synthetic route of the target diblock copolymer is shown in Scheme 1, and the procedure is similar to our previously reported procedure with slight modification.[46]

2.2.1 Preparation of PNMP homopolymers. PNMP homopolymers were prepared by RAFT radical polymerization in chloroform at 60 °C, which were purified by repeated precipitation in ethyl ether. The synthesized PNMP homologues were characterized by ^{1}H NMR spectroscopy and GPC, and the corresponding structural information is provided in the ESI Fig. S1 and Table S1.†

The detailed synthetic procedure is described as follows by taking PNMP$_{35}$ as an example. A 250 mL round-bottom flask was charged with NMP (50.0 g, 254 mmol), 2-cyano-2-propyl dithiobenzoate (CPDB, 1.52 g, 6.88 mmol), 2,2′-azobisisobutyronitrile (AIBN, 226 mg, 1.38 mmol, and the molar ratio of CPDB/AIBN = 5.0), and 52.5 mL chloroform. The sealed reaction vessel was purged with nitrogen for 30 min and placed in a preheated oil bath at 60 °C for 24 h. The resulting PNMP was purified by precipitation in excess ethyl ether. The degree of polymerization of the synthesized macro-CTA was calculated to be 35 using ^{1}H NMR spectroscopy, in which the integrated aromatic proton signals of CPDB at 7–8 ppm to the two oxymethylene PNMP protons at 3.7–4.2 were employed.

2.2.2 Synthesis of 1-ethenyl-4-(1,2,2-triphenylethenyl)-benzene (TPE). (2-Bromoethene-1,1,2-triyl)tribenzene (10.0 g, 29.9 mmol), 4-formylphenylboronic acid (5.30 g, 35.8 mmol),

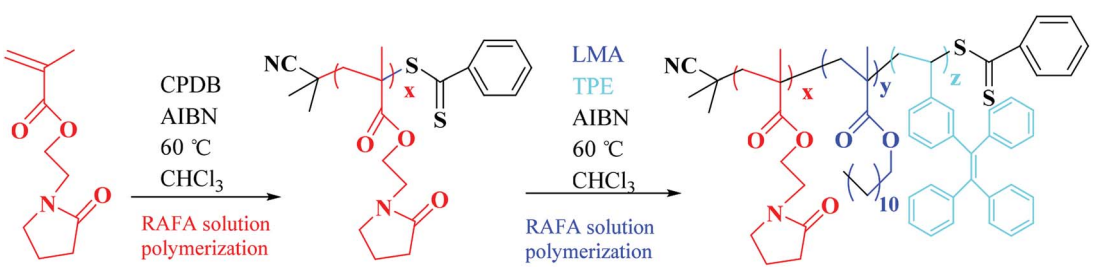

Scheme 1 Synthetic route of PNMP$_x$-*b*-P(LMA$_y$-*co*-TPE$_z$).

tetrabutylammonium tribromide (0.80 g, 1.66 mmol), 60.0 mL 2 M K_2CO_3 aqueous solution, and 250 mL toluene were added to the reaction vessel all at one time. The mixture was stirred at room temperature for 30 min under nitrogen protection, and then, 25.0 mg tetrakis(triphenylphosphine)palladium was added. The mixture was reacted at 85 °C for 24 h. After cooling, the crude product was extracted with CH_2Cl_2 and water in sequence. The organic phase was enriched and dried with anhydrous $MgSO_4$. Finally, a pure TPE product (4.98 g, yield 47%) was obtained by repeatedly conducting column chromatography using a silica gel column with petroleum ether as the eluent, which was characterized by ^{1}H NMR and mass spectra, as shown in the ESI Fig. S2 and S3,† respectively.

2.2.3 Synthesis of amphiphilic copolymers. The objective amphiphilic copolymers PNMP$_x$-*b*-P(LMA$_y$-*co*-TPE$_z$) were synthesized by RAFT solution polymerization with PNMP macro-CTA in chloroform at 60 °C and characterized by ^{1}H NMR spectroscopy and GPC, as shown in the ESI Fig. S4.†

The synthetic procedure of the PNMP$_{35}$-*b*-P(LMA$_{38}$-*co*-TPE$_{4.7}$) copolymer is typically described as follows. LMA (3.60 g, 14.2 mmol), TPE (0.51 g, 1.42 mmol), the AIBN initiator (11.5 mg, 0.07 mmol), and PNMP$_{35}$ macro-CTA (2.03 g, 0.28 mmol, and the molar ratio of macro-CTA/initiator = 4.0) were dissolved in 23.5 mL chloroform. The reaction mixture was sealed in a 50 mL round-bottom flask and purged with nitrogen gas for 30 min. The deoxygenated solution was then placed at 60 °C for 24 h. The resultant products were sequentially purified by dialysis against methanol and chloroform. The final sample was concentrated and dried in a vacuum oven at 25 °C for 12 h.

2.3 Preparation of PNMP-*b*-P(LMA-*co*-TPE) diblock copolymer assemblies

Self-assemblies in water were prepared by directly dissolving the copolymers (1 wt%) in water in an ice-water bath to achieve a 1 wt% aqueous solution. Similarly, self-assembles in alkane were prepared by directly dissolving the copolymers (1 wt%) in *n*-dodecane at 100 °C and then slowly cooling down the mixture to room temperature as previously reported.[46] To fully integrate PNMP$_{50}$-*b*-PLMA$_{10}$ with the AIE copolymers, these two substances were dissolved in the mixed solvent of methanol and THF, and then, dialysis was carried out to replace the organic solvent with water.

2.4 Characterization methods

2.4.1 Gel permeation chromatography (GPC). The GPC measurement was performed at 35 °C using chloroform as the eluent at the flow rate of 1.0 mL min^{-1}. The column set consisted of two 5 μm NZ-SD plus columns (500 Å and linear); the Wyatt Optilab DSP interferometric refractometer and the Wyatt DAWN EOS multiangle laser light-scattering detectors with a helium-neon laser light source (λ = 690 nm), K5 flow cell and a broad range of scattering angles from 45° to 160° were employed. A series of near-monodisperse polystyrene standards were used for calibration. The molecular weight and polydispersity data were determined using the Wyatt ASTRA software package. Polymer samples were prepared at the concentration of 20 mg mL^{-1} and filtered through a 0.22 μm nylon filter prior to analysis.

2.4.2 Nuclear magnetic resonance (NMR) spectroscopy. All ^{1}H NMR spectra were obtained *via* the 400 MHz Bruker Avance-400 spectrometer using $CDCl_3$.

2.4.3 Dynamic light scattering (DLS) measurements. The DLS measurements were performed using the Zetasizer instrument ZEN 3600 (Malvern, UK) with a 173° backscattering angle and He–Ne laser (λ = 633 nm) at 25 °C.

2.4.4 Transmission electron microscopy (TEM) observation. TEM was performed using the JEM-2100 TEM operated at the acceleration voltage of 200 kV. During the sample preparation process, the copolymer solution (0.2 wt%) was dropped on top of a carbon-coated copper grid and allowed to dry for 1 min, and then, excess solution was wicked off using filter paper. Assemblies in *n*-dodecane and water were stained by RuO_4 vapor[42] and the uranyl acetate aqueous solution (1 wt%),[41] respectively, before observation.

2.4.5 Fluorescence spectroscopy measurements. The fluorescent spectra were obtained using the Agilent G9800A fluorescence spectrometer with a 5 nm slit width and 600 nm min^{-1} scan rate. The excitation wavelength was set at 380 nm for all the samples.

2.4.6 Fluorescence quantum yield (QY) measurements. The absolute fluorescence quantum yield of the assemblies was measured using the FLS980 fluorescence spectrometer, and the excitation wavelength was set at 380 nm.

2.4.7 Confocal laser scanning microscopy (CLSM) observation. The morphology of the fluorescent assemblies (1 wt%) was characterized *in situ* by CLSM (PerkinElmer UltraVIEW VoX), and the laser diode (405 nm) was used as the excitation source.

2.5 Cytotoxicity measurements

The MTT (3-[4,5-dimethyl-2-thiazolyl]-2,5-diphenyl-2-*H*-tetrazolium bromide) assay was employed to evaluate the cytotoxicity of the complex against HeLa cells. At the density of 1×10^3 cells per well, the HeLa cells were placed in 96-well plates in 100 μL of DMEM (Dulbecco's modified Eagle medium). After 24 h, the previous medium was discarded, 200 μL of culture medium containing self-assemblies was added, and incubation was continued for 24 h in a cell incubator under the 5% CO_2 and 37 °C condition. Then, 20 μL of MTT solution (5 mg mL^{-1}) was put in a cell plate and continued to culture for 4 h; moreover, 150 μL of dimethyl sulfoxide was added to replace the culture medium. Finally, the absorbance was tested by a microplate reader (BioTek ELx800) at 490 nm.

2.6 Cell-imaging experiments

At the density of 2×10^3 cells per well, HeLa cells were put in a cell culture dish with the DMEM including 10% fetal bovine serum (FBS) and 1% antibiotics and incubated in a cell incubator under the 5% CO_2 and 37 °C condition. After culturing the cells for 24 h, the aggregates were cultured with the HeLa cells for 3 h and then washed three times with phosphate buffer saline (PBS). Images were obtained by CLSM at 400× magnification.

3 Results and discussion

3.1 Self-assembly of PNMP$_x$-*b*-P(LMA$_y$-*co*-TPE$_z$)

From the viewpoint of molecular structure, the PNMP$_x$-*b*-P(LMA$_y$-*co*-TPE$_z$) homopolymers are a typical category of amphiphiles, in which the PNMP and PLMA segments are the hydrophilic and hydrophobic parts, respectively, as mentioned previously.[46] Although the water-insoluble TPE moiety has only slight affinity to *n*-dodecane, the copolymers still exhibit excellent solubility in both water and *n*-dodecane by rationally adjusting the composition. In this study, five amphiphilic PNMP$_x$-*b*-P(LMA$_y$-*co*-TPE$_z$) copolymers were developed, and the detailed information is provided in Table 1. The polymerization degree of PNMP for all copolymers was kept constant at 35, indicating the same hydrophilicity. Therefore, their hydrophobicity should mainly depend on the polymerization degree of P(LMA$_y$-*co*-TPE$_z$), in which the ratio of *y*/*z* was kept nearly constant at about 9. Accordingly, the solubility of PNMP$_{35}$-*b*-P(LMA$_y$-*co*-TPE$_z$) in water was gradually weakened upon increasing the length of the P(LMA$_y$-*co*-TPE$_z$) segment. In contrast, the corresponding affinity to *n*-dodecane gradually increased from the copolymer No. 1 to No. 5.

3.1.1 Self-assembly of PNMP$_{35}$-*b*-P(LMA$_y$-*co*-TPE$_z$) in water.

It has been reported previously that PNMP-*b*-PLMA homologous

Table 1 Summary of the PNMP$_x$-*b*-P(LMA$_y$-*co*-TPE$_z$) copolymer composition, weight fraction of PNMP block, monomer conversion, and molecular weight determined by ^{1}H NMR and GPC

		PNMP	LMA	TPE	M_n (g mol^{-1})		M_w/M_n
Entry	Composition	Wt[a]	Conv.	Conv.	^{1}H NMR	GPC	GPC
No. 1	PNMP$_{35}$-*b*-P(LMA$_9$-*co*-TPE$_{0.9}$)	71%	81%	99%	9700	6300	1.10
No. 2	PNMP$_{35}$-*b*-P(LMA$_{18}$-*co*-TPE$_{1.9}$)	56%	86%	99%	12 400	8200	1.21
No. 3	PNMP$_{35}$-*b*-P(LMA$_{24}$-*co*-TPE$_{2.7}$)	50%	76%	99%	13 700	10 200	1.13
No. 4	PNMP$_{35}$-*b*-P(LMA$_{38}$-*co*-TPE$_{4.7}$)	37%	80%	99%	18 500	13 100	1.09
No. 5	PNMP$_{35}$-*b*-P(LMA$_{55}$-*co*-TPE$_{6.3}$)	30%	83%	99%	23 200	14 500	1.07

[a] Weight fraction of the PNMP block in the block copolymer.

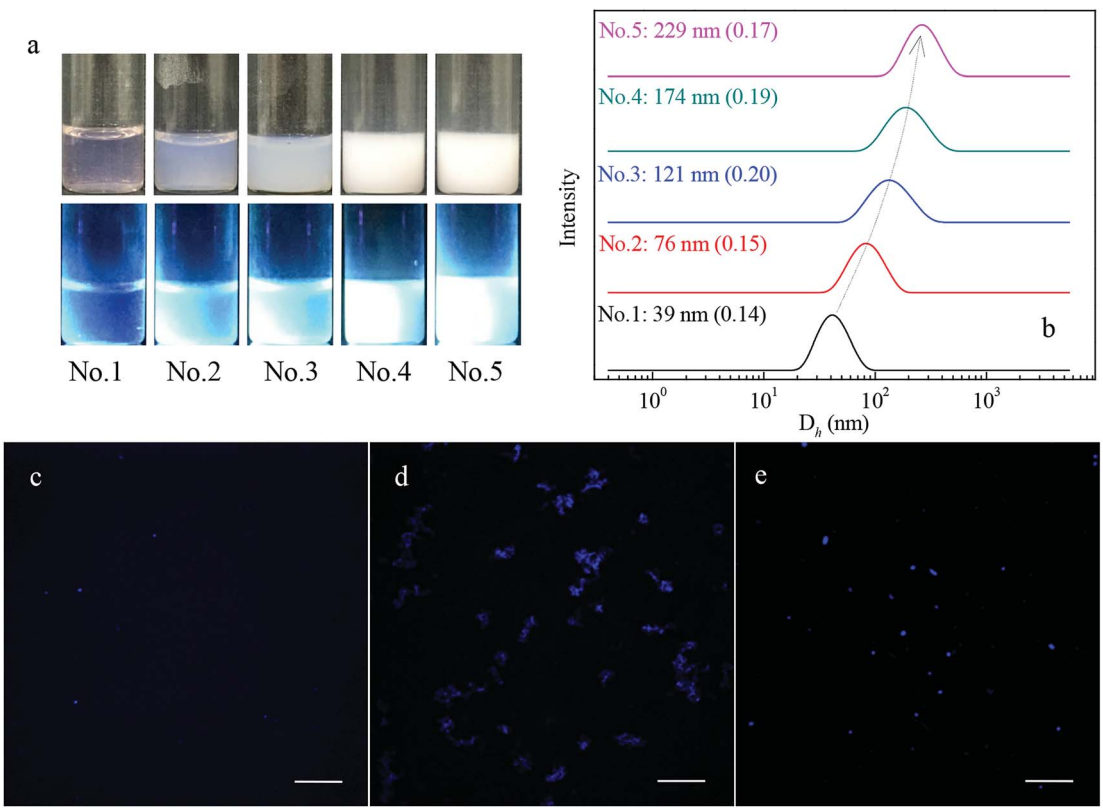

Fig. 1 Optical and fluorescence images (a) of 1 wt% PNMP$_{35}$-*b*-P(LMA$_y$-*co*-TPE$_z$) aqueous solution and the corresponding size distribution (b) of them. CLSM images of 1 wt% PNMP$_{35}$-*b*-P(LMA$_{18}$-*co*-TPE$_{1.9}$) (c), PNMP$_{35}$-*b*-P(LMA$_{24}$-*co*-TPE$_{2.7}$) (d) and PNMP$_{35}$-*b*-P(LMA$_{55}$-*co*-TPE$_{6.3}$) (e) aqueous solution. Bars represent 25 μm.

block copolymers mainly form self-organized assemblies in nonaqueous solvents.[45,46] We noticed that the newly developed $PNMP_{35}$-*b*-P(LMA_y-*co*-TPE_z) copolymers could also form structurally well-defined assemblies with rich morphologies in water. Since hydrophilicity originates from the hydrogen bond interaction between PNMP and water,[48] the chain length of the P(LMA_y-*co*-TPE_z) segment dramatically affects the assembly behaviors. Fig. 1a shows the optical (top) and fluorescence (down) images of the 1 wt% $PNMP_{35}$-*b*-P(LMA_y-*co*-TPE_z) aqueous solution. A gradual transition of the solution from being optically transparent to turbid was observed, and the fluorescence intensity was apparently enhanced upon increasing the length of the hydrophobic P(LMA_y-*co*-TPE_z) segment simultaneously. Dynamic light scattering (DLS) results of the 0.1 wt% $PNMP_{35}$-*b*-P(LMA_y-*co*-TPE_z) samples showed that the average hydrodynamic diameter (D_h) of the self-organized assemblies was increased from 39 nm to 229 nm with an increase in the length of the P(LMA_y-*co*-TPE_z) segment. This obviously suggested the formation of larger assemblies. These self-organized assemblies of different copolymers could be well distinguished based on the CLSM images, except for the case of $PNMP_{35}$-*b*-P(LMA_9-*co*-$TPE_{0.9}$) because of the low fluorescence resolution. It was also noticed that the morphologies of the assemblies of $PNMP_{35}$-*b*-P(LMA_{18}-*co*-$TPE_{1.9}$) and $PNMP_{35}$-*b*-P(LMA_{55}-*co*-$TPE_{6.3}$) were spherical, whereas that of $PNMP_{35}$-*b*-P(LMA_{24}-*co*-$TPE_{2.7}$) was linear corresponding to worm-like micelles.

To have a better understanding of the micro-structural characteristics of the assemblies, TEM measurements were also performed. Generally, a spherical micelle-to-vesicle transition *via* worm-like micelles occurred in the 1 wt% $PNMP_{35}$-*b*-P(LMA_y-*co*-TPE_z) aqueous solution upon increasing the length of the hydrophobic P(LMA_y-*co*-TPE_z) segment. Specifically, nearly spherical micelles of about 30–40 nm were formed in the $PNMP_{35}$-*b*-P(LMA_9-*co*-$TPE_{0.9}$) aqueous solution, and similar aggregates were also observed in the $PNMP_{35}$-*b*-P(LMA_{18}-*co*-$TPE_{1.9}$) (ESI Fig. S5a†) system. Instead, worm-like micelles and vesicles became the dominant morphologies for $PNMP_{35}$-*b*-P(LMA_{24}-*co*-$TPE_{2.7}$) and $PNMP_{35}$-*b*-P(LMA_{55}-*co*-$TPE_{6.3}$), as shown in Fig. 2b and c, respectively. Moreover, a binary mixture of worm-like micelles and vesicles was observed in $PNMP_{35}$-*b*-P(LMA_{38}-*co*-$TPE_{4.7}$) (ESI Fig. S5b†). Thus, TEM observation clearly confirms the morphological transition from spherical micelles to vesicles, and the increased hydrophobic chain is the major reason for the occurrence of this transition.[37]

3.1.2 Self-assembly of $PNMP_{35}$-*b*-P(LMA_y-*co*-TPE_z) in *n*-dodecane. As is known, *n*-dodecane is a good solvent for the homopolymer PLMA but a poor solvent for the PNMP segment, as previously reported;[46] therefore, $PNMP_{35}$-*b*-P(LMA_y-*co*-TPE_z) forms a self-assembly in this nonpolar solvent. Fig. 3a shows the optical (top) and fluorescence (down) images of $PNMP_{35}$-*b*-P(LMA_y-*co*-TPE_z) in *n*-dodecane at the concentration of 1 wt%, and a reverse transition tendency was observed when compared with that in the case of water (Fig. 1a). The samples were gradually transformed from being turbid to optically transparent upon increasing the polymerization degree of the P(LMA-*co*-TPE) segment. Moreover, the apparent fluorescence intensity was enhanced. The DLS results (Fig. 3b) show the size distribution of 0.1 wt% $PNMP_{35}$-*b*-P(LMA_y-*co*-TPE_z) in *n*-dodecane, in which the averaged value of D_h is decreased from 191 nm to 42 nm, indicating the formation of smaller aggregates. This was well-consistent with the macroscopic appearance of the samples.

Fig. 3c–e show the typical CLSM images of $PNMP_{35}$-*b*-P(LMA_9-*co*-$TPE_{0.9}$), $PNMP_{35}$-*b*-P(LMA_{18}-*co*-$TPE_{1.9}$) and $PNMP_{35}$-*b*-P(LMA_{55}-*co*-$TPE_{6.3}$) in *n*-dodecane, respectively, and distinguishable assemblies with different morphologies have been observed. Particularly, those of $PNMP_{35}$-*b*-P(LMA_{18}-*co*-$TPE_{1.9}$) and $PNMP_{35}$-*b*-P(LMA_{55}-*co*-$TPE_{6.3}$) seemed to be spherical dots dominantly, whereas that of $PNMP_{35}$-*b*-P(LMA_{24}-*co*-$TPE_{2.7}$) seemed to be rod-like particles. Their corresponding TEM images (Fig. 4) showed that vesicles were formed in the $PNMP_{35}$-*b*-P(LMA_9-*co*-$TPE_{0.9}$) *n*-dodecane dispersion. Alternatively, worm-like micelles and spherical micelles were formed in the $PNMP_{35}$-*b*-P(LMA_{18}-*co*-$TPE_{1.9}$) and $PNMP_{35}$-*b*-P(LMA_{55}-*co*-$TPE_{6.3}$) systems, respectively. In addition, the aggregate morphologies of $PNMP_{35}$-*b*-P(LMA_{24}-*co*-$TPE_{2.7}$) and $PNMP_{35}$-*b*-P(LMA_{38}-*co*-$TPE_{4.7}$) were confirmed to be worm-like micelles and spherical micelles, respectively, by the TEM observation (ESI Fig. S6†). Thus, it could be concluded safely that a vesicle-to-spherical micelle transition *via* worm-like micelles occurred upon increasing the length of the solvophilic P(LMA-*co*-TPE) segment.[46]

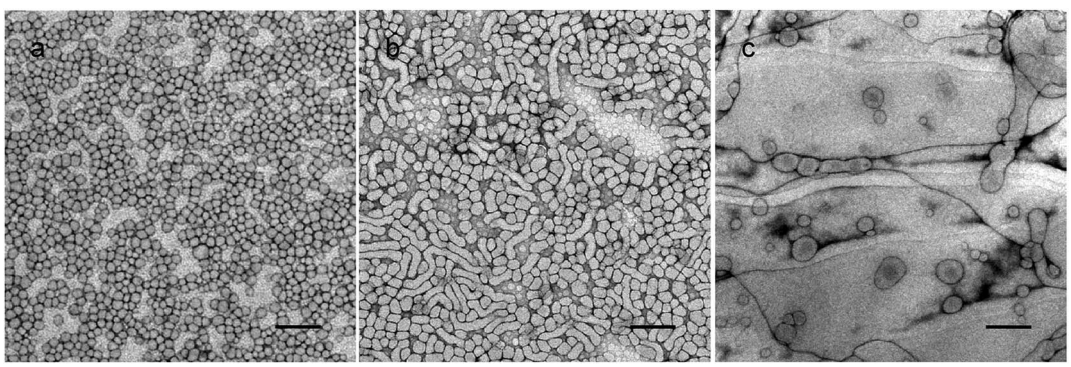

Fig. 2 TEM images of 1 wt% $PNMP_{35}$-*b*-P(LMA_9-*co*-$TPE_{0.9}$) (a), $PNMP_{35}$-*b*-P(LMA_{24}-*co*-$TPE_{2.7}$) (b) and $PNMP_{35}$-*b*-P(LMA_{55}-*co*-$TPE_{6.3}$) (c) aqueous solutions. Bars represent 200 nm.

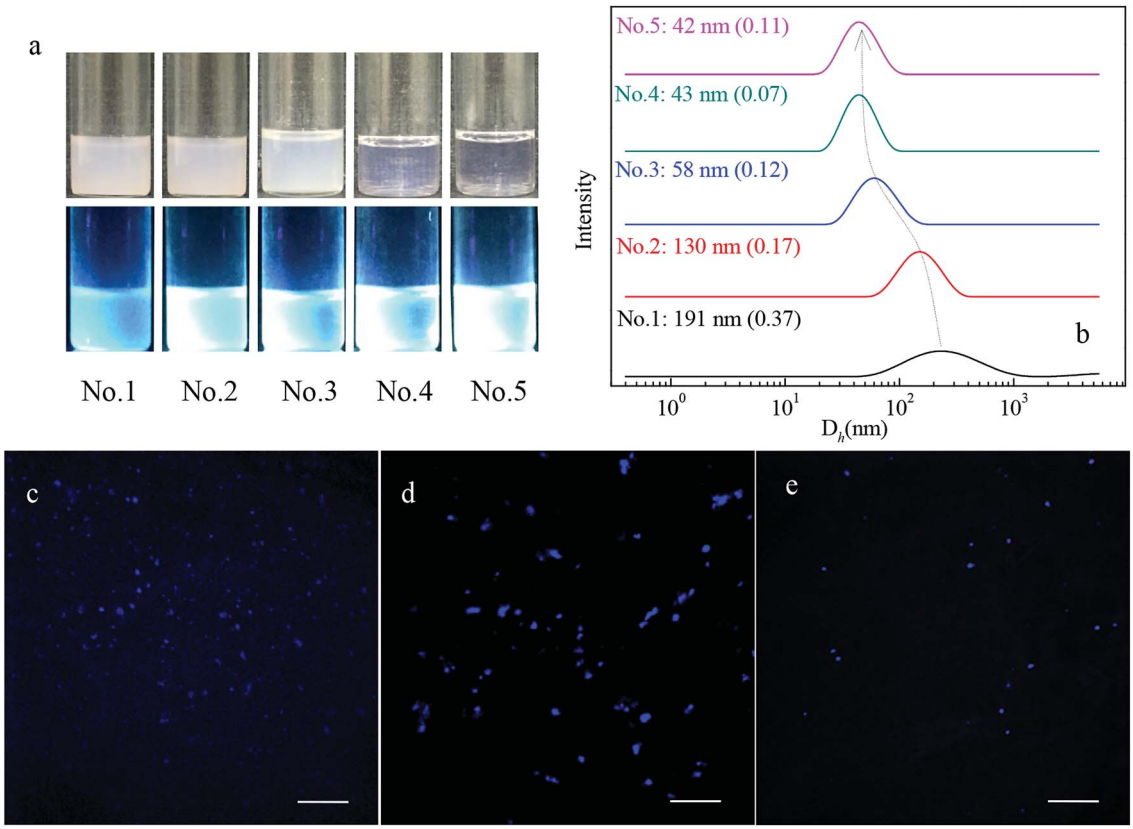

Fig. 3 Optical and fluorescence images (a) of 1 wt% PNMP$_{35}$-*b*-P(LMA$_y$-*co*-TPE$_z$) in *n*-dodecane and the corresponding size distribution (b). CLSM images of 1 wt% PNMP$_{35}$-*b*-P(LMA$_9$-*co*-TPE$_{0.9}$) (c), PNMP$_{35}$-*b*-P(LMA$_{18}$-*co*-TPE$_{1.9}$) (d) and PNMP$_{35}$-*b*-P(LMA$_{55}$-*co*-TPE$_{6.3}$) (e) in *n*-dodecane. Bars represent 10 μm.

3.2 Effect of self-assembly structure on AIE

One of the major specialties of PNMP$_{35}$-*b*-P(LMA$_y$-*co*-TPE$_z$) copolymers is the introduced TPE moieties, which endow them with aggregation-induced emission in either water (Fig. 1a) or *n*-dodecane (Fig. 3a), as observed from the fluorescence images. To clarify the AIE effect, the representative fluorescence spectra of 1 wt% PNMP$_{35}$-*b*-P(LMA$_{18}$-*co*-TPE$_{1.9}$) in water, *n*-dodecane and chloroform were examined, as shown in Fig. 5. Nearly no fluorescence characteristics could be observed from the chloroform solution. However, apparent fluorescence was observed in both the water and *n*-dodecane solutions. It was also noticed that the fluorescence intensity in *n*-dodecane was significantly stronger. This clearly suggested the aggregation-induced emission of PNMP$_{35}$-*b*-P(LMA$_{18}$-*co*-TPE$_{1.9}$) in the selected solvents. Since chloroform is a good solvent for both the PNMP and the P(LMA-*co*-TPE) segments, PNMP$_{35}$-*b*-P(LMA$_{18}$-*co*-TPE$_{1.9}$) is mainly present in its unimolecular form and shows a slight fluorescence. Instead, self-assemblies with different morphologies were formed in both water and *n*-dodecane, resulting in strong fluorescence.

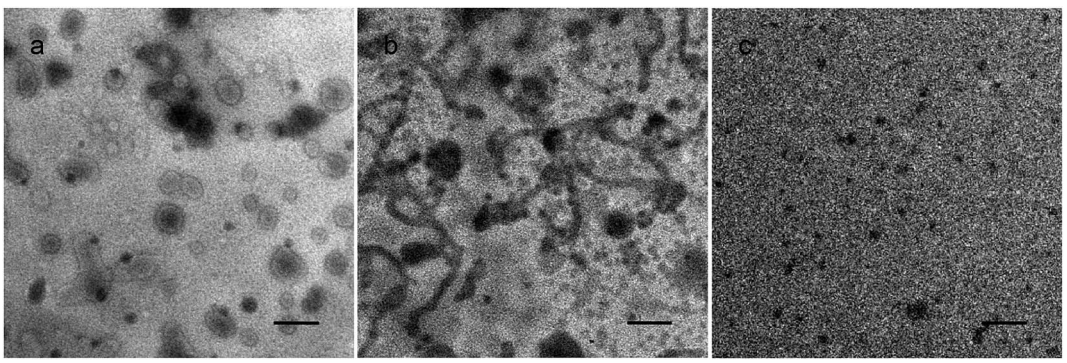

Fig. 4 TEM images of 1 wt% PNMP$_{35}$-*b*-P(LMA$_9$-*co*-TPE$_{0.9}$) (a), PNMP$_{35}$-*b*-P(LMA$_{18}$-*co*-TPE$_{1.9}$) (b), and PNMP$_{35}$-*b*-P(LMA$_{55}$-*co*-TPE$_{6.3}$) (c) in *n*-dodecane. Bars represent 200 nm.

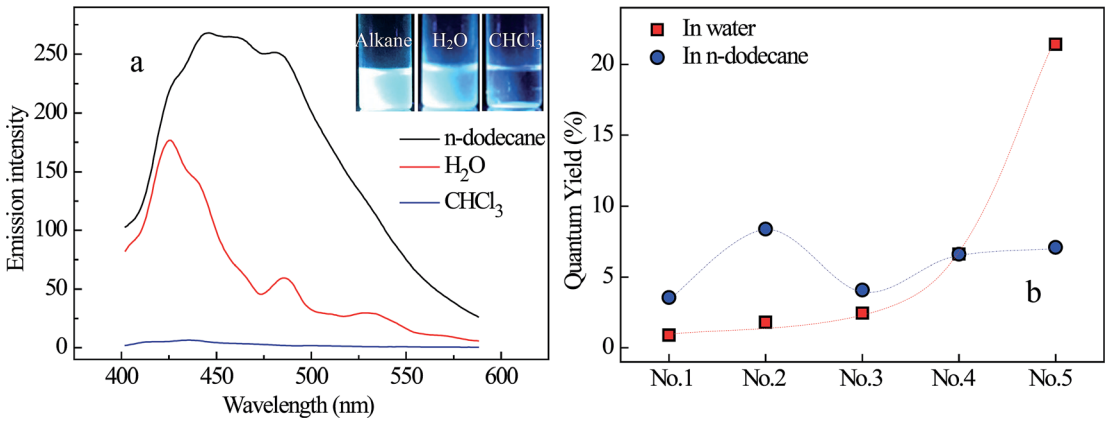

Fig. 5 (a) Fluorescence emission spectra of $PNMP_{35}$-*b*-P(LMA_{18}-*co*-$TPE_{1.9}$) in *n*-dodecane, water and chloroform; the inset images represent the corresponding fluorescence images. (b) Fluorescence quantum yield of $PNMP_{35}$-*b*-P(LMA_y-*co*-TPE_z) in water and *n*-dodecane with the constant concentration of 20 μg mL^{-1} for the TPE moiety.

Since there is a slight difference between the fluorescence responses of $PNMP_{35}$-*b*-P(LMA_y-*co*-TPE_z) in water and *n*-dodecane, the fluorescence quantum yields (QY) of both solutions have been measured, as shown in Fig. 5b. Clearly, the value of QY significantly depended on the nature of the solvent for a specific copolymer, and significantly different variation tendency was observed for $PNMP_{35}$-*b*-P(LMA_y-*co*-TPE_z) homologues in water and *n*-dodecane. In the aqueous solutions, all quantum yields of NMP_{35}-*b*-P(LMA_9-*co*-$TPE_{0.9}$), $PNMP_{35}$-*b*-P(LMA_{18}-*co*-$TPE_{1.9}$) and $PNMP_{35}$-*b*-P(LMA_{24}-*co*-$TPE_{2.7}$) were small, whereas those of $PNMP_{35}$-*b*-P(LMA_{38}-*co*-$TPE_{4.7}$) and $PNMP_{35}$-*b*-P(LMA_{55}-*co*-$TPE_{6.3}$) were significantly enhanced. Generally, the higher the polymerization degree of TPE, the larger the QY. Alternatively, the effect of polymerization degree on QY became more complex due to which the quantum yields of $PNMP_{35}$-*b*-P(LMA_y-*co*-TPE_z) in *n*-dodecane fluctuated in the region between about 3% and 9%. In addition, those with the averaged polymerization degree of TPE below 4.7 showed a larger QY in *n*-dodecane when compared with the case of water, whereas that of NMP_{35}-*b*-P(LMA_{55}-*co*-$TPE_{6.3}$) became smaller.

In addition to the effect of copolymer chain configuration on the QY of $PNMP_{35}$-*b*-P(LMA_y-*co*-TPE_z), QY should be mainly affected by the microstructural characteristics of the assemblies because of the constant concentration of the TPE moiety. Specifically, the morphology of the assemblies and the location of the TEP moieties in the assemblies were the major cause of the QY variation. In *n*-dodecane, the P(LMA-*co*-TPE) segment is the solvophilic part, which is solvated by *n*-dodecane regardless of the morphology of the assemblies. Accordingly, the effect of the assembly morphology on QY should be weakened dramatically because the micro-environment of the TPE moieties is kept nearly constant. However, the formation of large assemblies still favors the enhancement of QY. For example, large assemblies as vesicles were formed in $PNMP_{35}$-*b*-P(LMA_9-*co*-$TPE_{0.9}$), whereas its QY remained weak. The extremely small polymerization degree of the TPE moieties was the major cause, where the aggregation of the TPE moieties within a molecule by π–π interactions through the variation of copolymer configuration became difficult because of the solvation of the P(LMA-*co*-TPE) segment. Alternatively, a relatively larger QY was obtained

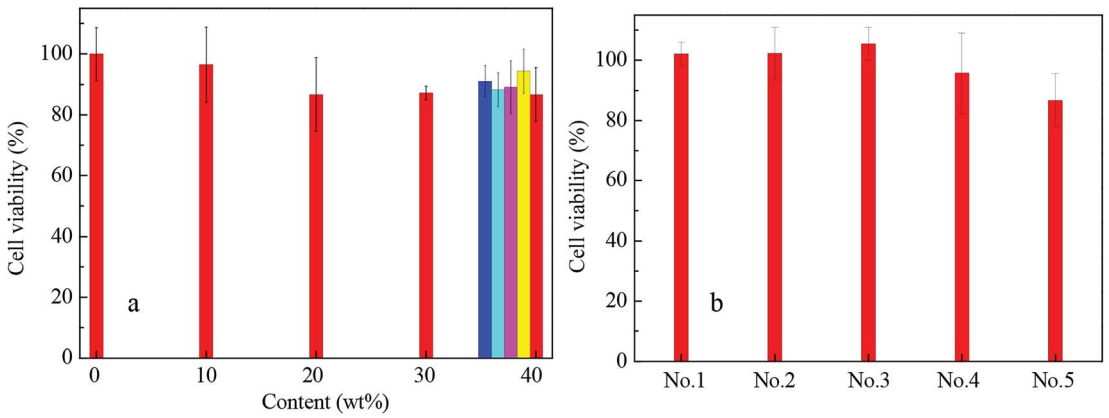

Fig. 6 Cell viability of the $PNMP_{35}$-*b*-P(LMA_y-*co*-TPE_z)/$PNMP_{50}$-*b*-$PLMA_{10}$ binary system with HeLa cells. (a) The effect of $PNMP_{35}$-*b*-P(LMA_{55}-*co*-$TPE_{6.3}$) content on the cell viability with a constant concentration of 100 μg mL^{-1}, and the effect of polymer concentration on the cell viability at the constant content of 40 wt% of $PNMP_{35}$-*b*-P(LMA_{55}-*co*-$TPE_{6.3}$). (b) The effect of copolymer structure on the cell viability with the constant concentration of 100 μg mL^{-1} and constant content of 40 wt% of $PNMP_{35}$-*b*-P(LMA_y-*co*-TPE_z).

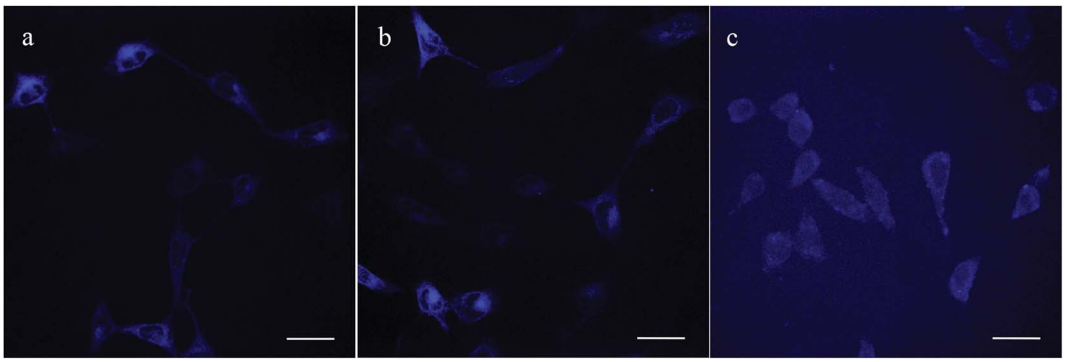

Fig. 7 CLSM images of the HeLa cells treated with $PNMP_{35}$-*b*-P(LMA_{24}-*co*-$TPE_{2.7}$) (a), $PNMP_{35}$-*b*-P(LMA_{38}-*co*-$TPE_{4.7}$) (b), and $PNMP_{35}$-*b*-P(LMA_{55}-*co*-$TPE_{6.3}$) (c). Bars represent 25 μm.

in $PNMP_{35}$-*b*-P(LMA_{18}-*co*-$TPE_{1.9}$) by slightly increasing the polymerization degree of the TPE moieties. This was because the formation of long and entangled worm-like micelles benefitted the aggregation of the TPE moieties within molecules and assemblies. Although a further increase in the polymerization degree of the TPE moieties was favorable, the formation of small assemblies, such as spherical micelles, became a disadvantage for the enhancement of QY, *i.e.*, $PNMP_{35}$-*b*-P(LMA_{55}-*co*-$TPE_{6.3}$) had smaller QY when compared with $PNMP_{35}$-*b*-P(LMA_{18}-*co*-$TPE_{1.9}$).

In the aqueous solution, the P(LMA-*co*-TPE) segment was always located in the hydrophobic core of the various assemblies regardless of the micelle or vesicle form. In other words, both the increased polymerization degree of TPE moieties and the formed assemblies of $PNMP_{35}$-*b*-P(LMA_y-*co*-TPE_z) should benefit the enhancement of QY. On the one hand, the formation of assemblies favors the aggregation of the TPE moieties and thereby increases the QY for a specific copolymer, as shown in Fig. 5a. The larger the assemblies, the higher the QY. Moreover, the increased polymerization degree of the TPE moieties benefitted the self-aggregation of copolymer chains within molecules, which was also favorable for the enhancement of QY. For copolymers, including $PNMP_{35}$-*b*-P(LMA_9-*co*-$TPE_{0.9}$), $PNMP_{35}$-*b*-P(LMA_{18}-*co*-$TPE_{1.9}$) and $PNMP_{35}$-*b*-P(LMA_{24}-*co*-$TPE_{2.7}$), with a relatively smaller polymerization degree of the TPE moieties, the QY values remained low because mainly small assemblies, such as spherical and rod-like micelles, were formed. In addition, a slight increase in the polymerization degree of the TPE moieties enhanced the QY. However, the QY values of $PNMP_{35}$-*b*-P(LMA_{38}-*co*-$TPE_{4.7}$) and $PNMP_{35}$-*b*-P(LMA_{55}-*co*-$TPE_{6.3}$) were increased dramatically due to the increased polymerization degree of the TPE moieties and the formation of large assemblies such as worm-like micelles and vesicles synergistically.

3.3 Cell imaging

As is well-known, one of the major advantages of pyrrolidone-containing chemicals is their excellent biocompatibility; therefore, they are widely applied in biological and drug delivery systems.[48] Due to the apparent fluorescence characteristics of the $PNMP_{35}$-*b*-P(LMA_y-*co*-TPE_z) copolymers based on the AIE, these copolymers might show promising potential in cell imaging. To weaken the biotoxicity of the TPE moiety in $PNMP_{35}$-*b*-P(LMA_y-*co*-TPE_z) and match the requirement of bioimaging, the biocompatible (Fig. 6a) and micelle-forming block copolymer $PNMP_{50}$-*b*-$PLMA_{10}$ (ESI Fig. S7†) was introduced. Fig. 6 shows the cell viability of the $PNMP_{35}$-*b*-P(LMA_y-*co*-TPE_z)/$PNMP_{50}$-*b*-$PLMA_{10}$ binary systems with HeLa cells as the objective substrate. Obviously, the biotoxicity (red columns in Fig. 6a) was enhanced upon increasing the content of $PNMP_{35}$-*b*-P(LMA_{55}-*co*-$TPE_{6.3}$) at the constant polymer concentration of 100 μg mL^{-1}, whereas over 85% cell viability was still retained when the content of $PNMP_{35}$-*b*-P(LMA_{55}-*co*-$TPE_{6.3}$) was increased to 40 wt%. Moreover, the cell viability varied slightly around 90% upon increasing the total copolymer concentration from 10, 25, 50, 75 to 100 μg mL^{-1} with the constant $PNMP_{35}$-*b*-P(LMA_{55}-*co*-$TPE_{6.3}$) content of 40 wt%, as shown by the blue to red columns. In addition, the cell viability was highly dependent on the AIE copolymers, and the increased polymerization degree of the TPE moieties was disadvantageous to the biocompatibility of these copolymers under the same conditions as shown in Fig. 6b. Generally, the larger the TPE concentration, the higher the biotoxicity.

Moreover, three AIE copolymers *i.e.* $PNMP_{35}$-*b*-P(LMA_{24}-*co*-$TPE_{2.7}$), $PNMP_{35}$-*b*-P(LMA_{38}-*co*-$TPE_{4.7}$) and $PNMP_{35}$-*b*-P(LMA_{55}-*co*-$TPE_{6.3}$) were employed in cell imaging, and micelles were commonly formed in the corresponding $PNMP_{35}$-*b*-P(LMA_y-*co*-TPE_z)/$PNMP_{50}$-*b*-$PLMA_{10}$ binary aqueous solutions with the constant $PNMP_{35}$-*b*-P(LMA_y-*co*-TPE_z) content of 40 wt% (ESI Fig. S8†). To ensure sufficient fluorescence and biocompatibility, the total copolymer concentration of 50 μg mL^{-1} was used. Fig. 7 shows the corresponding CLSM images of the HeLa cells in the presence of different AIE copolymers. Obviously, each cell could be distinguished clearly. However, the cells treated by $PNMP_{35}$-*b*-P(LMA_{24}-*co*-$TPE_{2.7}$) and $PNMP_{35}$-*b*-P(LMA_{38}-*co*-$TPE_{4.7}$) had much higher resolution than those treated by $PNMP_{35}$-*b*-P(LMA_{55}-*co*-$TPE_{6.3}$). The relatively higher biotoxicity of $PNMP_{35}$-*b*-P(LMA_{55}-*co*-$TPE_{6.3}$) (Fig. 6b) might be the major cause. Moreover, the microstructural characteristics of the cells shown in Fig. 7a and b were clearly presented. This evidently confirms that these AIE copolymers as probes clearly meet the requirements of bioimaging.

4 Conclusion

In summary, in this study, a series of AIE amphiphilic copolymers, namely poly(*N*-(2-methacryloyloxyethyl)pyrrolidone)-*b*-poly(lauryl methacrylate-*co*-1-ethenyl-4-(1,2,2-triphenylethenyl) benzene), $PNMP_x$-*b*-P(LMA_y-*co*-TPE_z), was developed by the RAFT polymerization method. Their corresponding self-assembly behaviors in both water and *n*-dodecane were studied systematically by employing the DLS, CLSM and TEM techniques. Accordingly, their structure–property relationships were illustrated well. Generally, an increase in the length of the P(LMA_y-*co*-TPE_z) segment with the ratio of *y*/*z* being around 9 enhanced the hydrophobicity of copolymers and thereby resulted in spherical micelle-to-vesicle transition *via* worm-like micelles in the aqueous solution. Instead, the reversed morphological transition from vesicles to spherical micelles *via* worm-like micelles occurred in *n*-dodecane because of the increased solvophilicity.[46] It was also noticed that the polarity of the solvent and the morphology of the assemblies significantly affected the apparent fluorescence quantum yields of $PNMP_{35}$-*b*-P(LMA_y-*co*-TPE_z), especially in the case of the aqueous solution. Although the introduced TPE moieties showed particular biotoxicity, the AIE-active amphiphilic copolymers could be potentially employed as excellent and highly efficient bioimaging probes under suitable conditions.[7]

Conflicts of interest

There are no conflicts to declare.

Acknowledgements

This work was supported by the National Natural Science Foundation of China (NSFC 21573164 and 21773174). The authors thank Prof. Yi Liu and Fenglei Jiang of Wuhan University for the measurements of cell imaging.

References

1 B. Liu, X. He, C. Xu, L. Xu, S. Ai, S. Cheng and R. Zhuo, *Biomacromolecules*, 2018, **19**, 2957–2968.
2 C. Liu, F. Xiong, H. Jia, X. Wang, H. Cheng, Y. Sun, X. Zhang, R. Zhuo and J. Feng, *Biomacromolecules*, 2013, **14**, 358–366.
3 M. Gong, J. Wu, B. Chen, R. Zhuo and S. Cheng, *Langmuir*, 2015, **31**, 5115–5122.
4 J. Li, Y. Cheng, C. Zhang, H. Cheng, J. Feng, R. Zhuo, X. Zeng and X. Zhang, *ACS Appl. Mater. Interfaces*, 2018, **10**, 5287–5295.
5 Y. Li, H. Cheng, Z. Zhang, C. Wang, J. Zhu, Y. Liang, K. Zhang, S. Cheng, X. Zhang and R. Zhuo, *ACS Nano*, 2008, **2**, 125–133.
6 G. Luo, X. Xu, J. Zhang, J. Yang, Y. Gong, Q. Lei, H. Jia, C. Li, R. Zhuo and X. Zhang, *ACS Appl. Mater. Interfaces*, 2012, **4**, 5317–5324.
7 Y. Zhao, Y. Wu, S. Chen, H. Deng and X. Zhu, *Macromolecules*, 2018, **51**, 5234–5244.
8 M. Huang, R. Yu, K. Xu, S. Ye, S. Kuang, X. Zhu and Y. Wan, *Chem. Sci.*, 2016, **7**, 4485–4491.
9 T. Jadhav, B. Dhokale, Y. Patil and R. Misra, *RSC Adv.*, 2015, **5**, 68187–68191.
10 T. Jadhav, B. Dhokale, S. M. Mobin and R. Misra, *J. Mater. Chem. C*, 2015, **3**, 9981–9988.
11 L. Viglianti, N. L. C. Leung, N. Xie, X. Gu, H. H. Y. Sung, Q. Miao, I. D. Williams, E. Licandro and B. Tang, *Chem. Sci.*, 2017, **8**, 2629–2639.
12 J. Luo, Z. Xie, J. W. Y. Lam, L. Cheng, H. Chen, C. Qiu, H. S. Kwok, X. Zhan, Y. Liu, D. Zhu and B. Tang, *Chem. Commun.*, 2001, 1740–1741.
13 J. Chen, C. C. W. Law, J. W. Y. Lam, Y. Dong, S. M. F. Lo, I. D. Williams, D. Zhu and B. Tang, *Chem. Mater.*, 2003, **15**, 1535–1546.
14 X. Fan, J. Sun, F. Wang, Z. Chu, P. Wang, Y. Dong, R. Hu, B. Tang and D. Zou, *Chem. Commun.*, 2008, 2989–2991.
15 S. Li, Q. Wang, Y. Qian, S. Wang, Y. Li and G. Yang, *J. Phys. Chem. A*, 2007, **111**, 11793–11800.
16 Y. Hong, J. W. Y. Lam and B. Tang, *Chem. Commun.*, 2009, 4332–4353.
17 J. Mei, Y. Hong, J. W. Y. Lam, A. Qin, Y. Tang and B. Tang, *Adv. Mater.*, 2014, **26**, 5429–5479.
18 Q. Peng, Y. Yi, Z. Shuai and J. Shao, *J. Am. Chem. Soc.*, 2007, **129**, 9333–9339.
19 T. Wu, J. Huang and Y. Yan, *Chem.–Asian J.*, 2019, **14**, 730–750.
20 M. Huo, Q. Ye, H. Che, X. Wang, Y. Wei and J. Yuan, *Macromolecules*, 2017, **50**, 1126–1133.
21 Z. Huang, X. Zhang, X. Zhang, S. Wang, B. Yang, K. Wang, J. Yuan, L. Tao and Y. Wei, *RSC Adv.*, 2015, **5**, 89472–89477.
22 Y. Zhao, Y. Wu, G. Yan and K. Zhang, *RSC Adv.*, 2014, **4**, 51194–51200.
23 Q. Zhou, C. Fan, C. Li, Y. Wang, Z. Chen, Q. Yu and M. Zhu, *Mater. Horiz.*, 2018, **5**, 474–479.
24 N. Zhang, H. Chen, Y. Fan, L. Zhou, S. Trépout, J. Guo and M. Li, *ACS Nano*, 2018, **12**, 4025–4035.
25 Y. Mai and A. Eisenberg, *Chem. Soc. Rev.*, 2012, **41**, 5969–5985.
26 K. Haraguchi, K. Kubota, T. Takada and S. Mahara, *Biomacromolecules*, 2014, **15**, 1992–2003.
27 A. Bousquet, E. Ibarboure, E. Papon, C. Labrugère and J. Rodríguez-Hernández, *J. Polym. Sci., Part A: Polym. Chem.*, 2010, **48**, 1952–1961.
28 Z. Liu, Y. Huang, X. Zhang, X. Tu, M. Wang, L. Ma, B. Wang, J. He, P. Ni and H. Wei, *Macromolecules*, 2018, **51**, 7672–7679.
29 Z. Wang, M. C. M. Oers, F. P. J. T. Rutjes and J. C. M. Hest, *Angew. Chem.*, 2012, **124**, 10904–10908.
30 P. Gu, C. Lu, F. Ye, J. Ge, Q. Xu, Z. Hu, N. Li and J. Lu, *Chem. Commun.*, 2012, **48**, 10234–10236.
31 X. Shen, Y. Shi, B. Peng, K. Li, J. Xiang, G. Zhang, Z. Liu, Y. Chen and D. Zhang, *Macromol. Biosci.*, 2012, **12**, 1583–1590.
32 X. Zhang, X. Zhang, B. Yang, M. Liu, W. Liu, Y. Chen and Y. Wei, *Polym. Chem.*, 2014, **5**, 356–360.
33 X. Zhang, X. Zhang, B. Yang, J. Hui, M. Liu, Z. Chi, S. Liu, J. Xu and Y. Wei, *Polym. Chem.*, 2014, **5**, 683–688.

34 X. Zhao, X. Fan, X. Chen, C. Chai and Q. Zhou, *J. Polym. Sci., Part A: Polym. Chem.*, 2006, **44**, 4656–4667.
35 Y. Miura and M. Okada, *Polymer*, 2004, **45**, 6539–6546.
36 J. Zhong, H. Luo, Q. Tang, Z. Lei and Z. Tong, *Macromol. Chem. Phys.*, 2019, **220**, 1800554.
37 H. Luo, Q. Tang, J. Zhong, Z. Lei, J. Zhou and Z. Tong, *Macromol. Chem. Phys.*, 2019, **220**, 1800508.
38 M. Semsarilar, N. J. W. Penfold, E. R. Jones and S. P. Armes, *Polym. Chem.*, 2015, **6**, 1751–1757.
39 D. Zehm, L. P. D. Ratcliffe and S. P. Armes, *Macromolecules*, 2013, **46**, 128–139.
40 V. Ladmiral, A. Charlot, M. Semsarilar and S. P. Armes, *Polym. Chem.*, 2015, **6**, 1805–1816.
41 Y. Pei, K. Jarrett, L. G. Garces, M. Saunders, J. Croue, P. J. Roth, C. E. Buckley and A. B. Lowe, *RSC Adv.*, 2016, **6**, 28130–28139.
42 M. J. Derry, L. A. Fielding and S. P. Armes, *Polym. Chem.*, 2015, **6**, 3054–3062.
43 J. Zhang, S. Cheng, X. Li and J. Dong, *Acta Phys.-Chim. Sin.*, 2016, **32**, 2018–2026.
44 S. Cheng, Y. Xue, Y. Lu, X. Li and J. Dong, *ACS Omega*, 2017, **2**, 105–112.
45 V. J. Cunningham, S. P. Armes and O. M. Musa, *Polym. Chem.*, 2016, **7**, 1882–1891.
46 X. He, X. Li and J. Dong, *Colloids Surf., A*, 2019, **577**, 493–499.
47 M. Benaglia, E. Rizzardo, A. Alberti and M. Guerra, *Macromolecules*, 2005, **38**, 3129–3140.
48 J. Sun, Y. Peng, Y. Chen, Y. Liu, J. Deng, L. Lu and Y. Cai, *Macromolecules*, 2010, **43**, 4041–4049.